



# POWER UP YOUR ANALYSIS

## Application solutions for lithium-ion secondary battery analysis

Lithium-ion secondary batteries with high-energy density are emerging as a new energy source. Materials for analyzing battery contents such as positive electrode materials, negative electrode materials, separators, and electrolytes are vital in research development and quality control.

To improve battery characteristics and safety, it's essential to understand the internal state of the battery through multiple analyses. Explore our application solutions for lithium-ion secondary battery analysis that combine analytical instruments such as FT-IR, ICP-OES, GC/MS, and DSC.



Learn more at  
[www.perkinelmer.com/battery](http://www.perkinelmer.com/battery)



# Operation of a Solid Oxide Fuel Cell Reactor with Multiple Stacks in a Pressured System with Fuel Gas Recirculation

Marius Tomberg,\* Marc Philipp Heddrich, Matthias Metten, Syed Asif Ansar, and Kaspar Andreas Friedrich

Large-scale modular solid oxide fuel cell (SOFC) reactors composed of multiple stacks are regarded as an efficient form of power generation and important for the global energy transition. However, such an arrangement leads to several operational challenges, and methods are required for handling such challenges and understanding their sources. Hence, a test rig for the examination of a 30 kW SOFC reactor with multiple stacks, for operation near real system conditions, is built. The test rig, which allows operation at elevated pressure, is equipped with a high-temperature blower that recirculates the fuel gas at SOFC reactor temperature. In a measurement campaign, fuel gas, reactant conversion, and pressure are varied in stationary and transient experiments. The experimental results showed that the operating conditions of the individual stacks of large SOFC reactors vary largely due to flow distribution and heat losses. Methods for the investigation of these critical characteristic parameters are derived from the experimental results. Furthermore, the impact of pressurization and fuel gas recirculation on the SOFC reactor is analyzed. This publication shows the need to understand the behavior of large SOFC reactors with multiple stacks to increase the performance and robustness of complete process systems.

## 1. Introduction

Solid oxide cells (SOCs) are flexible and efficient energy conversion devices. In solid oxide fuel cell (SOFC) mode, they can efficiently convert chemical into electrical energy. Due to the high operating temperature and the stable catalysts, the cells can cope with various fuels based on hydrogen and reformed

hydrocarbons. However, to play a significant role in the future energy system, SOFCs need to reach the megawatt and multi-megawatt range. This can be achieved partly by significantly increasing the active cell area and the current density, but at a certain point, this will be limited by technological and manufacturing barriers. Therefore, megawatt reactors are expected to be designed as modular reactors with multiple sub-reactors in the near future.<sup>[1,2]</sup>


Pressurization of SOFCs can provide several benefits to further increase the impact of this technology. First, it has a positive impact on Nernst voltage and reaction kinetics, leading to a higher reactor efficiency.<sup>[3]</sup> Second, the overall system efficiency can be increased in combination with a gas turbine cycle.<sup>[4]</sup> Fuel gas recirculation provides heat and hot steam for reforming of hydrocarbons<sup>[5]</sup> and can increase the system fuel conversion.

However, there are only few scientific publications on operation of large reactors with multiple stack towers. For example, Gandiglio et al.<sup>[6]</sup> examined large SOFC reactors in a biogas-fed plant, and Nether et al.<sup>[7]</sup> investigated a large SOFC reactor for maritime application. However, both do not examine the operating behavior of the individual stacks. Srikanth et al.<sup>[8]</sup> published heat-up and pressure loss experiments on a 4-stack SOFC reactor. Aicart et al. did a performance evaluation of a 4-stack solid oxide reactor though mostly in electrolysis mode.<sup>[9]</sup> Operation under elevated pressures has been investigated by several research groups (e.g.,<sup>[10–14]</sup>) for single stacks but not for reactors with multiple stack towers. Experiments with recirculation blowers were investigated with cooled recirculation gases<sup>[15]</sup> and for systems with only a single stack.<sup>[16]</sup> Research focusing on the behavior of SOFC reactors with multiple stacks in process systems with BoP components is needed to support scaling of SOFC reactors into the megawatt and multi-megawatt range.

Therefore, a large SOFC reactor with multiple stack towers was examined under pressurized conditions within a 30 kW SOFC system (**Figure 1**), which was built at the German Aerospace Center (DLR) in Stuttgart, Germany. In addition to pressurized operation, this system was equipped with a high-temperature blower for direct fuel gas recirculation at SOFC reaction temperature as well as an array of integrated sensors, such as thermocouples and voltage measurements, to monitor values

M. Tomberg, M. P. Heddrich, M. Metten, S. A. Ansar, K. A. Friedrich  
Institute for Engineering Thermodynamics  
German Aerospace Center (DLR)  
70569 Stuttgart, Germany  
E-mail: marius.tomberg@dlr.de

K. A. Friedrich  
Institute for Building Energetics  
Thermotechnology and Energy, Storage  
University of Stuttgart  
70569 Stuttgart, Germany

 The ORCID identification number(s) for the author(s) of this article can be found under <https://doi.org/10.1002/ente.202101075>.

© 2022 The Authors. Energy Technology published by Wiley-VCH GmbH. This is an open access article under the terms of the Creative Commons Attribution License, which permits use, distribution and reproduction in any medium, provided the original work is properly cited.

DOI: 10.1002/ente.202101075

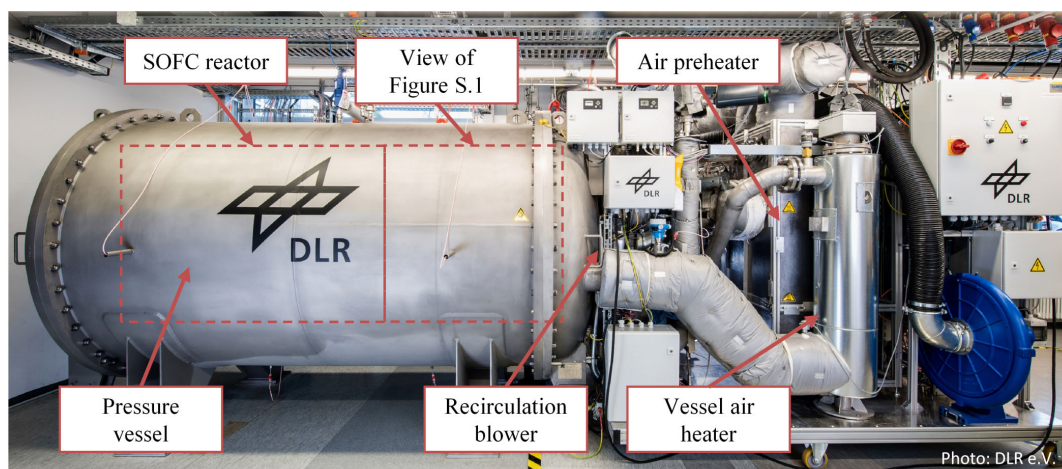


**Figure 1.** Solid oxide fuel cell (SOFC) system with a 30 kW reactor built and operated at German Aerospace Center (DLR) in Stuttgart. The image was adapted with permission from the German Aerospace Center (DLR).

throughout the test rig and the reactors. These features make the system one of its kind and a highly sophisticated setup for the scientific investigation of SOFC reactors.

In this work, the behavior of an SOFC reactor with many stacks in a system context was studied. This was done in two steps. First, the reactor was examined, which consists of several sub-reactors and thus allows investigating the challenges of future modular megawatt reactors. The main factors, including heat losses and unequal flow distribution, which result in different temperature and reactant conversion rates within the multitude of stacks, were analyzed in detail. In the second step, the impact of the surrounding system components on the individual cells and stacks was investigated. The results showed that this impact cannot be neglected and it is rather important for the design and operation of systems using SOFC reactors.

The experimental setup is described in Section 2. Section 3 focuses mostly on the operational behavior of the SOFC reactor

and its multiple stacks. Subsequently, effects resulting from the particular structure of the investigated system are analyzed (Section 3.3). In Section 4, the findings are summarized and future research steps are described.

## 2. Experimental Setup

In this work, the behavior of an SOFC reactor with multiple stacks, which was operated in a system, was investigated. For this purpose, a unique test rig was designed and built by the DLR containing an SOFC reactor with 48 stacks. All subcomponents were purchased from suppliers or developed together with them. In most cases, these were tailor-made products for the test bench or products in the commercialization phase that have a high degree of novelty. The Supporting Information contains additional material about the setup.

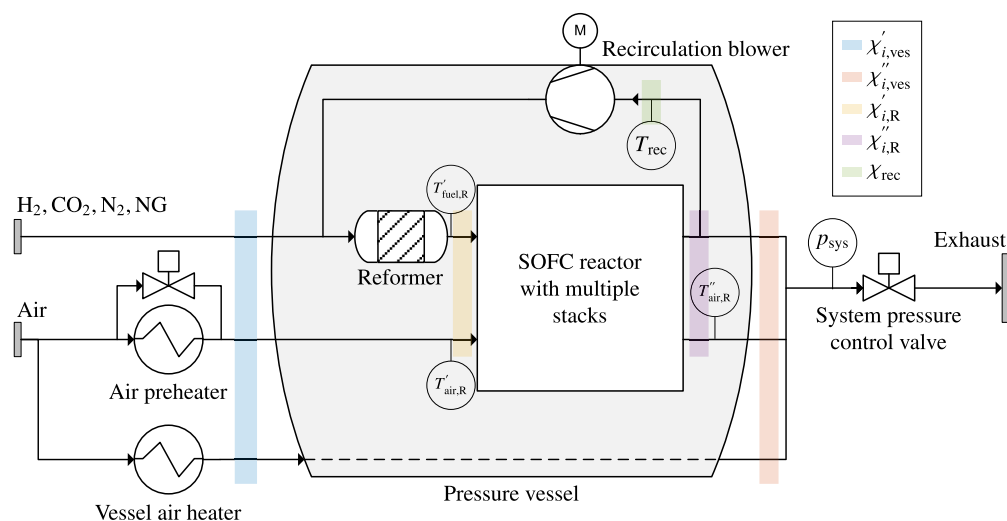


**Figure 2.** Simplified piping and instrumentation diagram of the pressurized SOFC test rig. The colored areas show the locations described by the indices “ves,” “R,” and “rec,” which indicate vessel inlet and outlet, reactor inlet and outlet, as well as the recirculation flow. The natural gas (NG) is desulfurized. Inlet values are marked with a single apostrophe (') and outlet values with a doublet ('').

Figure 2 shows a simplified piping and instrumentation diagram of the test rig. For the sake of simplicity, it contains only the sensors, actors, and pipes relevant for this publication. The fuel gas, which can consist of hydrogen, carbon dioxide, nitrogen, and natural gas (NG), entered the vessel and was mixed with the recirculation flow. After leaving the steam reformer, it flowed through the SOFC reactor. Before leaving the vessel, the product gas was partly recirculated. The reactor air flow was preheated before entering the SOFC reactor, and the vessel air flow was used to purge and pressurized the vessel. All flows were mixed and the pressure was controlled using the system pressure control valve.

### 2.1. SOFC Reactor with Multiple Stacks

The reactor consisted of 1440 commercially available electrolyte-supported cells, grouped in 48 stacks. The 30 cells per stack had an active area of 127.8 cm<sup>2</sup> each and were designed for co-flow operation. The 55 mm thick oxygen electrodes consisted of lanthanum strontium cobalt ferrite oxide (LSCF) and the 30 mm thick fuel electrode of nickel gadolinia-doped ceria (Ni-GDC). The electrolyte was approximately 90 mm thick and consisted of 3 mol% yttria-stabilized zirconia (3 YSZ). In addition, there was a GDC layer between the electrolyte and the fuel electrode as well as between the electrolyte and the air electrode. More detailed information about the cells and their composition could be obtained from Riedel et al.<sup>[14]</sup> Figure 3 shows the internal architecture of the SOFC reactor in the xz and the xy plane. It consists of six sub-reactors (SR A-F). Each sub-reactor was formed by two towers (front tower F and back tower B) with four stacks each (stack level 1–4). The stacks in one sub-reactor shared a common air compartment.

The six sub-reactors were connected to one air and one fuel flow distribution pipe in parallel forming the SOFC reactor. Apart from the sensors shown in Figure 2, the overall voltage of the stack was measured via voltage taps on the endplates. Thus, not individual cell voltages but average cell voltages were measured. Additionally, thermocouples measured the air temperature at the outlet of the center cell of each stack  $T''_{\text{stack}}$ . The stacks were named after their location (e.g., the stack on the second level in the front tower of sub-reactor D is called D2F). The right part of Figure 3 shows the fuel distribution inside the sub-reactors. The flow entered the sub-reactors through the bottom of the sub-reactors and was distributed to

the cells by the internal manifold of each stack tower. The sub-reactors were insulated with respect to each other and the environment by high-temperature insulation materials. The sensors and power cables were led through at the bottom of the sub-reactors into a combined sensor compartment. The target sensor compartment's temperature must remain below 80 °C and was controlled by an additional cooling air flow.

### 2.2. Balance of Plant Components

The outlet fuel gas of the SOFC reactor was directly recirculated at reaction temperature with a blower delivering heat and product gases to the steam reformer in front of the SOFC reactor. The reformer outlet temperature was approximately equal to the SOFC reactor inlet temperature. The air was preheated before entering the SOFC reactor by a gas burner via a heat exchanger. Both the air and the fuel gas flow were mixed before passing through a valve that controls the system pressure. The system pressure  $p_{\text{sys}}$  could be adjusted between 1 and 4.5 bar. The electrical currents of the six sub-reactors could be controlled separately. A second air flow, whose temperature is controlled by an electric preheater, pressurized the vessel. This allowed the temperature around the reactor to be changed. The fuel could be a mixture of hydrogen, desulfurized NG, carbon dioxide, and nitrogen. Each gas flow was controlled by an individual mass flow controller. The test rig was built with respect to the later investigation of the coupling of an SOFC with a micro gas turbine into a Hybrid Power Plant (HyPP).<sup>[17]</sup> Therefore, certain boundary conditions were limited as some components were built to emulate the behavior of a gas turbine. For example, the preheating of the air flow was limited to the maximum temperature that can be achieved by recuperating the heat from the exhaust gases of the emulated gas turbine. The recirculation blower SSR-70 was developed for gas at reactor temperature of SOFC systems by the company CAP Co., Ltd.<sup>[18]</sup> and its rotational speed  $\omega_{\text{rec}}$  was controlled by a variable-frequency drive (VFD), which has a maximum speed of 44 400 rpm. However, the maximum speed was limited to 42 000 rpm to avoid damage of the bearings in long-term operation. Additional information on the blower is available in the Supporting Information section, by the manufacturer<sup>[19]</sup> and in a project report.<sup>[20]</sup> The power electronics had six channels, each connected to a sub-reactor. The electrical current could be inverted and fed into the grid or, in case of grid instabilities, dissipated via resistor banks. The test

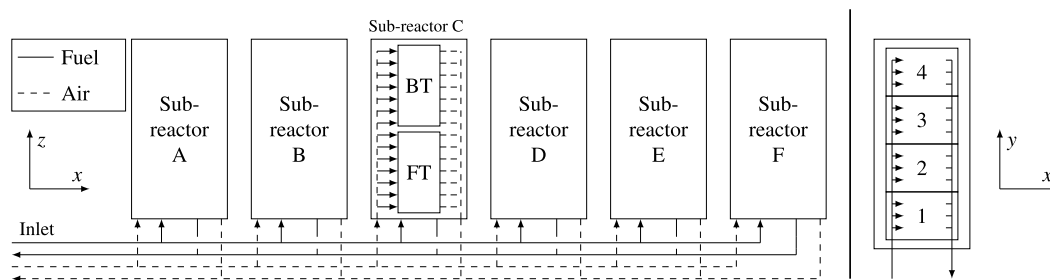


**Figure 3.** Simplified flow diagram of the internal flows in the SOFC reactor (xz-plane). Sub-reactor C shows the internal air flow to the front tower (FT) and back tower (BT) through one common air chamber. All sub-reactors have the same internal design. Simplified flow diagram of the internal fuel flows in each sub-reactor containing two towers with four stacks each (xy-plane).

rig was controlled by a control system, which is described in Sections 3.1 and S.4 (Supporting Information).

### 3. Results

The results section is divided into three parts. First, the developed control system is presented, which was the basis for all experiments. Second, the behavior of the SOFC reactor with multiple stacks and, third, the behavior of the whole system was investigated.

#### 3.1. System Control

To perform the necessary experiments on the 30 kW SOFC system, a control scheme was developed and implemented. It was derived from the control scheme of the HyPP presented by Henke et al.<sup>[21]</sup> and later described by Marcellan et al.<sup>[22]</sup> This was done by using additional controllers due to the additional degrees of freedom. For example, in case of direct coupling of SOFC and gas turbine (SOFC partially replaces the combustion chamber), the pressure of the SOFC reactor is determined by the cooling air mass flow and thus the pressure ratio of the compressor. Since there is no compressor, the pressure must be adjusted by an additional controller. Further information is available in the Supporting Information. During the experiments, the system was controlled by a programmable logic controller (PLC) mostly using PI controllers. The most important controllers are described as follows: 1) Power controller: This closed-loop controller modulates the nominal current  $I_{nom}$  until the set value of the electrical DC power  $P_{el,DC, set}$  is reached. A protection mechanism is implemented to avoid too high cell temperatures and too low cell voltages; 2) Load controller: This loop controller assigns currents to the individual sub-reactors  $I_{SR i}$  depending on a given distribution key. It must apply  $I_{nom} = 1/n_{SR} \sum_{i=A} I_{SR i}$  with  $n_{SR}$  as the number of sub-reactors; 3) Fuel mass flow controller: Open-loop controller that calculates the mass flows of the individual fuel components (hydrogen, NG, nitrogen, carbon dioxide) depending on the set values for system reactant conversion and fuel composition; 4) Reactor temperature controller: Closed-loop controller that controls the maximum reactor temperature  $\max(T''_{stack})$  by varying the air mass flow  $\dot{m}'_{air,R}$ ; 5) Fuel gas inlet temperature controller: Closed-loop controller that controls the fuel gas inlet temperature  $T_{fuel,R}$  into the SOFC reactor with the recirculation blower speed  $\omega_{rec}$  as manipulated variable. It must be ensured that there is always enough product flow for steam reforming; and 6) System pressure controller: Closed-loop controller that controls the system pressure  $p_{sys}$  using the pressure control valve.

The controllers were parameterized using the step response method and tuning rules based on Ziegler and Nichols<sup>[23]</sup> during commissioning. Additional information on these tuning rules were presented by Åström and Murray.<sup>[24]</sup> More sophisticated techniques such as gain scheduling and feed forward approaches were used if needed. Unless noted otherwise, this controller configuration was used in all the experiments shown hereafter.

#### 3.2. Analysis of SOFC Reactor Operation with Multiple Stacks

The performance of SOFC cells and stacks is usually characterized by current, voltage, temperature, input gas composition, and reactant conversion. In this work, it was investigated whether the characterization using these parameters of operating points is also adequate for SOFC reactors with multiple stacks. In the first step, stationary operating points were compared and critical parameters were identified. In the second step, the performance of the individual stacks was closely examined.

##### 3.2.1. Comparison and Analysis of Stationary Operating Points

During the experiments, several stationary operating points were obtained. In this section, five representative operating points were investigated extensively, which are detailed in Table 1. It is explained which parameters prevent a further increase in power or efficiency, and which parameters reach their limits. In general, the reasons are different temperatures and voltages of the individual stacks, which, in combination with the electrical connections, lead to a limitation of the overall performance.

Apart from the measured parameters, the following calculated parameters were used: the system reactant conversion  $X_{sys}$  was calculated using fuel flow and electrical current. The recirculation rate is defined as the ratio of recirculated mass flow and SOFC reactor gas outlet mass flow  $\dot{m}_{rec}/\dot{m}'_{fuel,R}$ . The SOFC reactor reactant conversion  $X_R$  (single pass) can be calculated as a function of recirculation rate and system reactant conversion  $X_{sys}$ .

$$X_R = \frac{X_{sys} \left( 1 - \frac{\dot{m}_{rec}}{\dot{m}'_{fuel,R}} \right)}{1 - X_{sys} \frac{\dot{m}_{rec}}{\dot{m}'_{fuel,R}}} \quad (1)$$

In this work, the fuel is defined as the ratio of the chemical power of the NG flow  $P_{ch,NG}$  and the total (NG and H<sub>2</sub>) flow  $P_{ch,tot}$ . The calculation is based on the lower heating values (LHVs).

$$\frac{P_{ch,NG}}{P_{ch,tot}} = \frac{\dot{m}'_{NG,ves} \text{LHV}_{NG}}{\dot{m}'_{fuel,ves} \text{LHV}_{fuel}} \quad (2)$$

These operating points were chosen because they represent characteristic reactor behavior, namely load variation, NG variation, and oxygen utilization, and each can be used to analyze a specific effect. Furthermore, the test rig was operated in these points for at least 10 h to rule out transient effects.

Operating point 1 was obtained during the first manual heat-up, which was interrupted during the night. It was chosen as it is a stationary out-of-spec operating point depicting the performance at low temperatures. However, the system reactant conversion was already near 90% resulting in system gross efficiency of  $\eta_{gross,LHV} = P_{el,DC}/P_{ch,tot} = 53.8\%$ . Due to the low average stack voltage, the current was not increased to prevent cell damage (cf. Section 3.3.1). Operating point 2 had the highest NG share in the fuel gas of the stationary operating points. This resulted in a high recirculation rate and a low air mass flow. Therefore, the minimum cell voltage was close to its limit. This relationship is discussed in more detail in Sections 3.3.3 and 3.3.4. Operation points 3–5 achieved a high system gross efficiency of nearly 60%.

**Table 1.** Average measured values of the solid oxide fuel cell (SOFC) reactor for five stationary operating points.

Operating point	OP		1	2	3	4	5
Electric power	$P_{el,DC}$	kW	9.30	19.5	19.0	19.0	25.0
Current density	$j$	$A\ cm^{-2}$	0.07	0.14	0.14	0.14	0.18
Average cell voltage	$U_{cell}$	V	0.759	0.737	0.74	0.743	0.738
Minimum cell voltage	$U_{min}$	V	0.74	0.682	0.692	0.695	0.685
Average stack outlet temperature	$T''_{stack}$	$^{\circ}C$	788.4	830.2	828.8	828	834.9
Maximum stack outlet temperature	$T''_{stack,max}$	$^{\circ}C$	831.3	850.3	850	850	855.7
System pressure	$p_{sys}$	bar	1	2	2	2.4	3
System reactant conversion	$X$	%	88	89	89	89	70
Natural gas (NG) lower heating value share	$P_{ch,NG}/P_{ch,tot}$	%	0	72	50	50	0
Oxygen utilization	$OU$	%	16.1	32.1	27.6	30.4	25.7
Air reactor inlet temperature	$T'_{air,R}$	$^{\circ}C$	713.4	707.3	701.9	700.6	633.8
Fuel reactor inlet temperature	$T'_{fuel,R}$	$^{\circ}C$	659.3	650	650	650	650
Recirculation rate	$\dot{m}_{rec}/\dot{m}_{fuel,R}$	%	71	84	81	81	74
System gross efficiency	$\eta_{gross,LHV}$	%	53.8	60.0	57.8	58.0	41.0

The three operation points had a high reactant conversion, elevated pressure, and an NG share of at least 50%. The operation points 3 and 4 differ only in pressure. These were chosen to investigate the pressure impact including a transient ramp in Section 3.3.2. The highest electrical power of the stationary operating points was achieved with a system reactant conversion of 70% (OP5) and pure hydrogen as fuel. Further power increase is limited by the voltage limit. According to the reactor's specification, the temperature difference between fuel inlet temperature and stack temperature must not exceed 200 °C. To minimize the load of the recirculation blower, the fuel inlet temperature  $T'_{fuel,R}$  was set to 650 °C, which is the lower limit at  $T''_{stack} = 850$  °C.

All operating points in Table 1 showed low average stack outlet temperatures  $T''_{stack}$  and high average cell voltages. In contrast, the maximum individual stack outlet temperatures and the minimum cell voltages were near their set points (e.g., OP5:  $T_{Max} = 850$  °C and  $U_{Min} = 0.7$  V). The average cell voltages of the weakest stacks were 30 to 50 mV lower than the average cell voltage of all stacks. As the stacks per sub-reactor are electrically connected in series, this spread of the observed parameters leads to low average current densities. The current density cannot be increased without exceeding the set values for the maximum temperature or the minimum voltage.

This shows that the usage of the average values does not give any indication on the spread of the parameters and the operability of the reactor. Therefore, it is necessary to observe not only the average values of the SOFC reactor but also the operational parameters of all its stacks as each stack operates under different operating conditions. This is mostly due to an uneven distribution of temperature and flows in the SOFC reactor because of the geometrical arrangement of the stacks, which causes different heat losses and different flows in the individual stacks as shown in Sections 3.2.2 and 3.3. To increase power and performance, the applied operation strategy must consider these effects. Therefore, **Figure 4** is used to examine the locations and operating conditions of the critical stacks.

The figure depicts each stack by a box. The colors of the individual stacks represent the stack temperatures and the average cell voltages (in volt) are written inside the boxes. The stacks on the bottom level have a much lower temperature than the stacks on the top level. In the sub-reactors B to F, the stacks x4B have the highest temperature (as far as measured). In sub-reactor A, it is stack A3B. The back towers tend to have higher temperatures than the front towers. This may be due to air preheating and uneven distribution in the inlet air chamber or higher heat losses as the pipes interrupt the heat insulation at

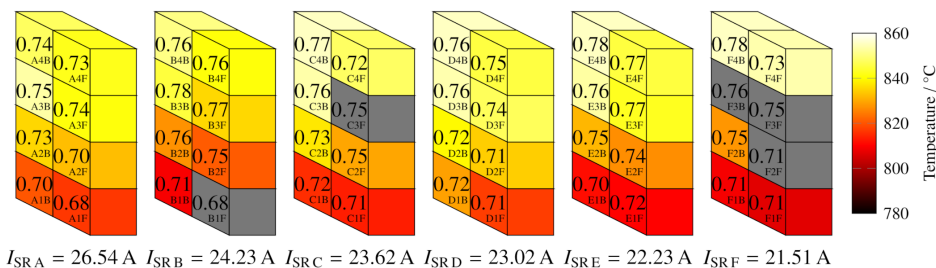


**Figure 4.** Temperatures (color mapped) and average cell voltages (written inside boxes in volt) of the individual stacks in the SOFC reactor for operating point 6. Gray boxes indicate broken thermocouples. The thermocouples measure the air outlet temperature of the center cell of each stack.

the front towers. Furthermore, the electrical currents of the sub-reactors were modified in such a way that temperatures of the sub-reactors were homogenized. Without this adaption of the electrical currents, the temperature of the first stack would be much too low while the temperature of the last one would be too high. This is due to the increasing pressure loss along the x-axis of the SOFC reactor, which leads to higher air flows through the first sub-reactors. The average cell voltages seem to be influenced by the temperatures (higher voltages at the top cells) and the current (lower voltages at the first sub-reactors). This correlation is further examined in Section 3.2.2. The electrical DC power at this operating point is  $P_{el,DC} = 25.0$  kW while  $P_{el,AC} = 23.6$  kW were fed into the grid with a power electronics efficiency of 94.4%. Assuming that all stacks would behave as the best and the worst stack, respectively, the electrical power would be  $P_{el,DC} = 28.6$  kW and  $P_{el,DC} = 22.0$  kW.

The difference in power between best and worst performing stack was 26.4% of the average stack power. This section showed that it is difficult to compare operating points because the inter-relationships are difficult to determine. Different heat and pressure losses lead to an uneven distribution of the gas flows and different temperatures of the individual stacks. An analysis of the average values of the SOFC reactor's operating parameters is thus not sufficient. Therefore, in Section 3.2.2, the performance of the individual stacks is examined in detail.

### 3.2.2. Performance

As proposed in Section 3.2.1, the performance of the individual stacks is evaluated in this section. Assuming a uniform flow distribution, the area-specific resistance (ASR) was used to evaluate the performance of the individual stacks, considering the local temperatures and flows. Subsequently, this and other assumptions are examined for their applicability. The ASR is defined as the difference in measured voltage  $U_{measured}$  and conversion rate-dependent ideal voltage  $U_{id}$  divided by the current density  $j$ .

$$ASR = \frac{U_{id} - U_{measured}}{j} \quad (3)$$

The ideal voltage  $U_{id}$  was calculated using the Nernst equation assuming ideal gases ( $a_i = p_i/p_0$ ). Moreover, by assuming the

stacks to be zero dimensional, these can be treated as a continuous stirred-tank reactor. Therefore, the average composition  $\bar{x}_i = 0.5(x'_i + x''_i)$  between inlet ('') and outlet ('') was used.<sup>[14,25]</sup>

$$U_{id} = U_0 + \frac{RT}{zF} \ln \left( \frac{\bar{x}_{H_2} \bar{x}_{O_2}^{0.5}}{\bar{x}_{H_2O}} \left( \frac{p}{p_0} \right)^{0.5} \right) \quad (4)$$

Figure 5 shows the ASR of the individual stacks for the stationary operating points 1–6. Two assumptions had to be made. First, the fuel and air flows were assumed to be equal for each stack.

$$\dot{m}'_{stack,i} = \frac{1}{n_{stacks}} \dot{m}'_r \quad (5)$$

Second, each stack outlet temperature  $T''_{stack}$  was assumed to be the characteristic temperature of its corresponding stack.

$$ASR_{stack,i} = ASR(T''_{stack,i}) \quad (6)$$

The black line shows the ohmic part of the ASR according to Riedel et al.<sup>[14]</sup> The red fitting function takes all ASR values into account using the same model function. The values of the sub-reactors A and B seem to be smaller than those of the fitting function while the values of the sub-reactors E and F are larger. Furthermore, if a quadratic fitting function is chosen instead, it will have a minimum around 850 °C. This is due to the high-calculated ASR of the stacks that are mainly located in tower levels 3 and 4.

To investigate these behaviors, the values were plotted against their stacks' locations in Figure 6. With an increasing distance from the SOFC reactor inlet (SR A→F), the measured ASR was increasing. In combination with the shown current distribution (Figure 4), this led to the conclusion that the calculated ideal voltage had to be wrong as the flow distribution was not equal. It is likely that the sub-reactors further away from the air and fuel gas inlets had higher local reactant conversions and thus higher electrochemical losses. For further investigation, stepwise corrections were made to explain the experimental results. By subtracting the local values of the fit function (in Figure 5), the ASR values became temperature corrected ([I], red). The values were still increasing with the distance from the SOFC reactor inlet.

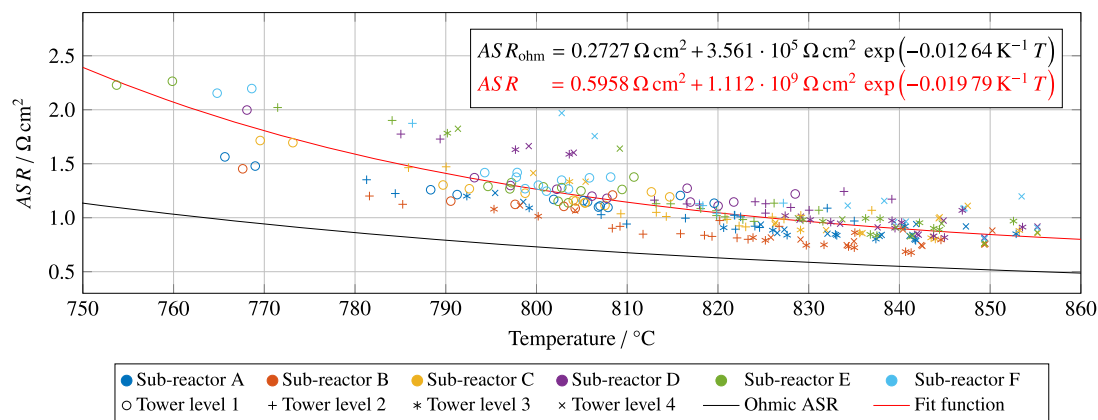
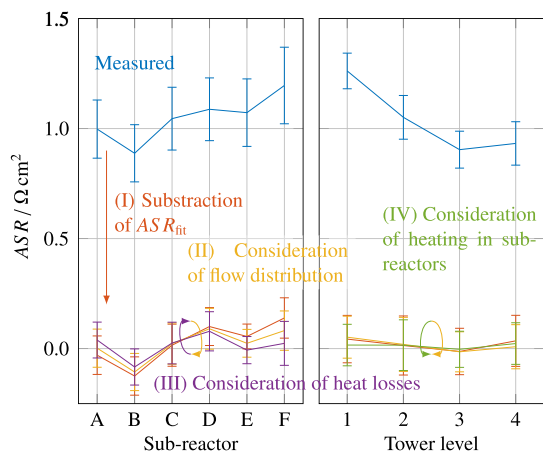


Figure 5. Area-specific resistance (ASR) of the individual stacks plotted against the stack temperature. An even flow distribution is assumed.



**Figure 6.** ASR plotted against their stacks' locations. It was assumed that the volume flow distribution through the sub-reactors is linear. In the calculation, sub-reactor A received 25% more flow than the average and sub-reactor F 25% less (II). Furthermore, it was assumed that difference between the characteristic and the average cell temperature of the stacks in sub-reactor F is 10 K smaller than in sub-reactor A, due to heat losses in the pipe feeding the sub-reactors (III). The vertical fuel and temperature distribution was considered to behave similarly. In the calculation, the lower stacks received 10% more fuel gas and the top stacks received 10% less (II) while the lower stacks' characteristic temperature was presumed to be 5 K colder than the measured one (IV). The position of the towers (front or back) does not have a significant influence and is therefore omitted in this analysis.

Two further corrections were applied. First, an unequal flow distribution was assumed (II, yellow). Second, the measured stack exit temperatures were assumed to be the characteristic stack temperature. The differences between characteristic and measured temperature were varied as the heat losses in the inlet pipes cause different stack inlet temperatures (III, purple). With these assumptions, the final curve was nearly horizontal, which means that all sub-reactors had a similar performance. Within the small variation, sub-reactor B had the lowest ASR while sub-reactor D had the highest.

The reverse trend can be observed over the height of the towers. The higher the stack's position in the tower (levels 1→4), the lower its calculated ASR. It is obvious that this was due to the vertical temperature spread (I). However, small deviations from zero are still present in the red plot. These can be explained by the temperature increase in the fuel manifold of each stack tower (cf. Figure 3). With increasing height in a stack tower, the inlet temperature was increasing. Therefore, the axial temperature difference between cell inlet and outlet decreased as does the difference between the characteristic and the measured temperature (IV). It has to be considered that several other parameters probably had an influence. These are for example heat losses of the sub-reactors into the vessel volume or the sensor compartment. Probably, the outer sub-reactors (A and F) had higher heat losses, which will change the temperature profile. Furthermore, the outer stacks per tower (1 and 4) may also have had higher heat losses. The diagrams show indications of these effects. This section showed that the temperature, the temperature profile, and the local reactant conversion of the individual stacks varied

strongly. Therefore, a performance characterization of an SOFC reactor with multiple stacks that is only using average or maximal values can never be exact and extensive. Instead, the steps (II)–(IV) shown in this manuscript can be used to interpret the measured values.

The authors propose as a result of this part of the investigation, a variation of several parameters, such as fuel and oxygen conversion, and subsequent analysis with the diagrams shown to investigate the impact of these parameters. For further analysis and the determination of characteristic values, simulation models for SOFC reactors with multiple stacks including pressure losses, heat losses, etc., should be developed. In contrast to the works of Li et al.,<sup>[26]</sup> Navasa et al.,<sup>[27]</sup> and Kim et al.,<sup>[28]</sup> not only the processes within a single stack but also the interaction between different stacks should be analyzed and explained by these numeric models.

### 3.3. Analysis of System Operation

While the Section 3.2.2 referred mostly to the SOFC reactor, this section examines matters that arise from the characteristics of this particular system setup.

#### 3.3.1. Start-up of the System

SOFC reactors must be heated up by an external source until ionic conductivity allows for additional heating using the polarization resistances. For the startup of the system described here, an air preheater consisting of a gas burner and a heat exchanger are used as an external source (Figure 2). In combination with the bypass valve, the air inlet temperature  $T'_{\text{air,R}}$  can be controlled. To reduce the risk of cell damage, three conditions must be considered during heat-up. 1) The maximum temperature difference between air inlet temperature and reactor temperature (250 K); 2) The maximum temperature difference between fuel gas inlet temperature and reactor temperature (200 K); and 3) The maximum temperature difference between fuel gas inlet temperature and air inlet temperature (150 K).

This is ensured by controlling the inlet temperatures via the blower speed and the preheater power respectively the bypass valve position. During startup, the limiting factor was the difference between the inlet temperatures. As there is no fuel preheater in this setup, the fuel gas inlet temperature can only increase along with the temperature of the SOFC reactor and its outlet flow temperature. The heat-up was automated respecting these temperature limits.

Having reached average reactor temperatures above 650 °C, the ionic conductivity of the deployed cell type allows for additional heating using the polarization resistances. Additionally, the upper limit of external heating is reached at  $T'_{\text{air,R}}$  of around 720 °C for this particular system setup.

As the reactor temperature is far below nominal, even low current densities lead to high overpotentials resulting in the desired heat-up. Figure 7 depicts the beginning of power generation. The process can be divided into different phases (1–6) that are shown in Figure 7. 1) Enthalpy flow difference between the inlets and outlets of the SOFC reactor were equal to the SOFC reactor's heat losses; 2) Cells were far below



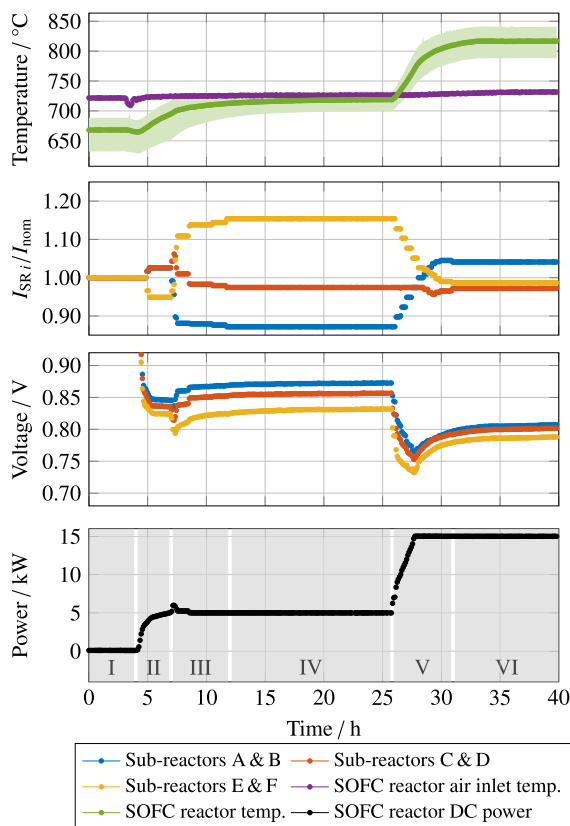


**Figure 7.** Start-up of the system using different currents for the sub-reactors. In interest of clarity, the sub-reactors are grouped. The temperature plot depicts the minimum, average, and maximum temperature of all stacks inside the SOFC reactor.

operation temperature. Sub-reactors E and F could not generate much heat. Therefore, the currents of the sub-reactors E and F were reduced and the others were set to a higher value (see  $I_{SR,i}/I_{nom}$  plot). Minimum cell voltage was set to 0.8 V to reduce the risk of damaging the top or bottom cells of the cold stacks, which were likely to have an even lower temperature; 3) At  $t = 7$  h, the load of the sub-reactors E and F was slowly increased to bring them to the same temperature level as the other stacks. The currents of the sub-reactors A and B were reduced, as their temperatures were already quite high; 4) No set point changes during night; 5) At  $t = 26$  h, the power was increased to 15 kW, and the temperature controller was activated subsequently. The higher air mass flow cools the sub-reactors A and B more than the sub-reactors E and F due to the flow distribution. Therefore, currents of sub-reactors A and B were increased and the currents of sub-reactors E and F were decreased. This switch is also visible in the temperature plot. During the switch, the temperature spread between the stack with the highest and the one with the lowest temperature became much smaller; and 6) Subsequently, all controllers were activated and the system was operational.

The described heating strategy is system specific and was automated using the aforementioned steps.

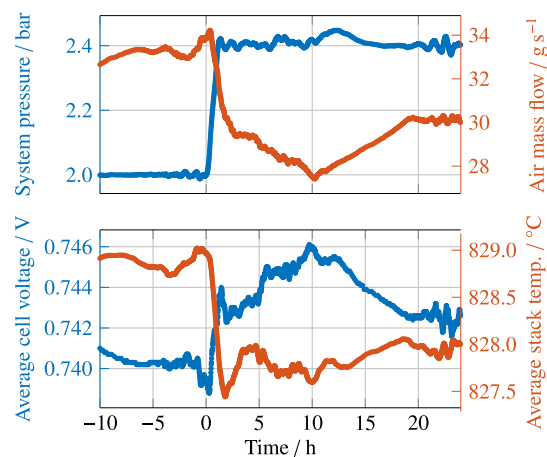


**Figure 8.** Impact of increasing pressure on the system's operation parameters.

### 3.3.2. Effects of Pressurization

Pressurization of SOCs is often aimed at in literature to improve kinetics and thus cell performance.<sup>[3,12,29]</sup> Additionally, the SOFC operation mode is also thermodynamically favored because of the increase in voltage. This section shows that for the investigated system, the effects on heat transfer counterbalance this partly. **Figure 8** shows experimental data of a step change in system pressure.

At  $t = 0$  h, the set value of the system pressure was increased from 2.0 to 2.4 bar within 1 h. As operating temperature drops immediately, the reactor temperature controller reduces the air mass flow. When the system returns to steady-state 20 h after the pressure ramp, the air mass flow was around 10% lower, which cannot be explained exclusively by a higher efficiency but by a significant increase in heat losses. It was found that the heat transfer of the insulation materials is pressure dependent, namely increasing proportionally. In addition, the recirculation mass flow was increased because the heat losses of the recirculation pipe, the blower, and the reformer increased.

The minimum and the average voltage increased by 2.2 mV. To investigate this further, the impact of the observed parameters on the ideal voltage was investigated. The influence of pressure on polarization losses can be neglected for this cell type as Riedel et al.<sup>[30]</sup> showed. Considering only pressure increase with the Nernst equation, the ideal voltage increases by 4.3 mV. Additionally, considering the aforementioned changes in air mass flow and recirculation, the ideal voltage increases by only 3 mV. This leads to the conclusion that the anticipated positive impact of pressure on the electrochemical performance is impeded by the reduction of the average temperature, lower Nernst potential due to a higher recirculation mass flow, and higher oxygen utilization.

To verify the impact of pressure on the heat losses, these were plotted as a function of the system pressure in **Figure 9** for a wide range of operating parameters. The heat losses were calculated as follows, using the enthalpy flows  $\dot{H}$  around the vessel.

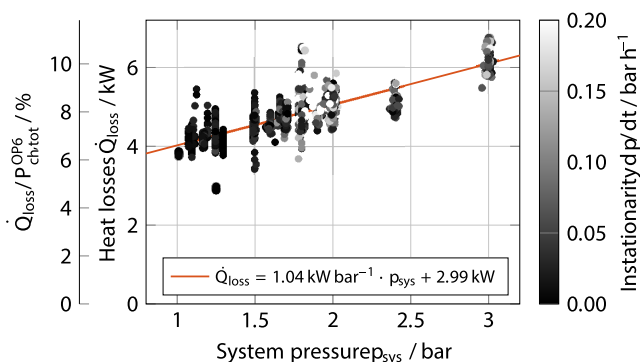


**Figure 9.** Impact of system pressure on the heat losses from the SOFC reactor and the recirculation line to the vessel air flow and the ambient. The heat losses are related to the chemical input power of operating point 6. The linear fit is calculated by weighting the operating points by stationarity.

$$\dot{Q}_{\text{loss}} = \dot{H}'_{\text{air,ves}} - \dot{H}''_{\text{air,ves}} + \dot{H}'_{\text{fuel,ves}} - \dot{H}''_{\text{fuel,ves}} + P'_{\text{ch,tot}} X_{\text{sys}} - P_{\text{el}} \quad (7)$$

An approximately linear correlation can be seen from the fit. A similar behavior was also reported by Brabandt and Posdziech.<sup>[31]</sup> It can be explained by thermal conduction in the fluid phase of the used microporous insulation. The thermal conduction of the fluid phase is a function of pressure,<sup>[32,33]</sup> as it depends on the mean free path  $l$ .<sup>[3,33,34]</sup> It can be concluded that pressurization not only enhances cell performance but also increases heat losses of the system. In addition, for this system, the average temperature decreases, the Nernst potential decreases, and the oxygen utilization increases. A next-generation test rig should invest in more or better suited insulation. It must be determined for each system whether the efficiency gain is high enough to justify the investment costs for a pressurized system. The use of electrode-supported cells can increase not only the efficiency gain but also increase the operational risk due to the lower mechanical stability.<sup>[30]</sup> Alternatively, other insulation concepts or materials can be developed.

### 3.3.3. Cooling of the SOFC Reactor

The temperature of the SOFC stacks is only measured at the air outlet (see Section 2.1). The air mass flow controls the maximum stack temperature (see Section 3.1). However, due to the recirculation, the fuel gas flow and its cooling effect are considerably larger compared to systems without recirculation. The impact of this high flow and thus the high cooling effect on the fuel side are analyzed.

**Figure 10** shows the dependency of several operating parameters on the NG share in the fuel gas for stationary operating points with a system reactant conversion of over 80%. For each parameter, a linear fit is plotted into the figure. The cooling potential  $\Delta \dot{H}_{i, \text{cooling potential}}$  is defined as the difference in the enthalpy flow between inlet and outlet assuming mass flow and composition are constant over the reactor with  $i$  representing fuel gas or air.

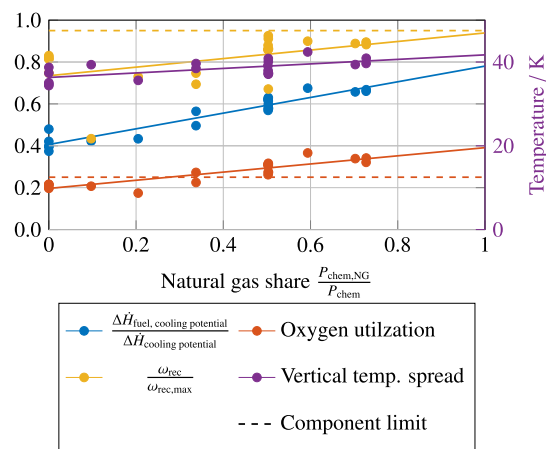


**Figure 10.** Impact of NG in the fuel on the cooling ratio between fuel and air, the oxygen utilization, and the recirculation blower speed, as well as the average vertical temperature spread ( $T_{x4z} - T_{x1z}$ ).

$$\Delta \dot{H}_{i, \text{cooling potential}} = \dot{m}'_i h_i(T'_i, x'_i) - \dot{m}''_i h_i(T''_i, x''_i) \quad (8)$$

The enthalpy  $h$  is calculated as a function of the local temperature  $T$  and gas composition  $x$  without considering the standard enthalpies of formation. The fuel flow cooling potential share correlates approximately linearly with the NG share (based on the LHV) in the fuel gas as the steam reforming reaction needs more heat resulting in a higher recirculation mass flow. Extrapolation of the corresponding linear fit to 100% NG leads to a fuel side cooling share of 80%. This reduces the air flow even further and increases the oxygen utilization, which exceeds its limit of 25% already at around 30% NG. Furthermore, the higher recirculation mass flow requires a higher recirculation blower speed or a higher pressure. Therefore, the recirculation blower speed  $\omega_{\text{rec}}$  is always near its limit. Another effect of this is the increasing average vertical temperature spread ( $T_{x4z} - T_{x1z}$ ).

In summary, for this particular system setup, the following consequences were identified. First, the air mass flow becomes ever smaller, which means that oxygen utilization exceeds its limit resulting in a lower Nernst potential, higher diffusion overpotentials, and thus lower operating voltages. The diffusion impact was probably small due to the thin electrodes<sup>[35,36]</sup> but will increase in case of electrode-supported cells. Second, the vertical temperature gradients increased further due to the greater cooling at the fuel gas electrode and the uneven preheating over the height of the stack towers. All in all, the operating range was decreasing with a higher NG share. Section 3.3.4 identifies the individual steps that provide remedy in certain situations.

### 3.3.4. Impact on Operability

This section describes the limitations in operability arising from the combination of fuel gas recirculation at reaction temperature, steam reforming, and pressurization described in the preceding section. This is done using the scheme in **Figure 11**, which also identifies the steps that can be taken to stabilize an operating point. When the share of NG in the fuel  $x_{\text{fuel,NG}}$  is increased,

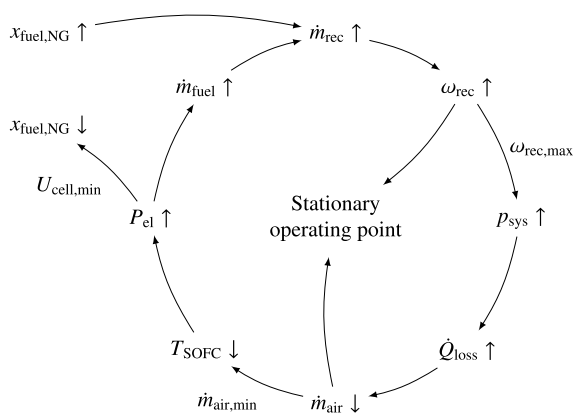


**Figure 11.** Impact of system pressure and NG on operability. The process starts with an increase of the NG share in the fuel  $x_{\text{fuel,NG}}$ .

the fuel inlet temperature  $T''_{\text{fuel,R}}$  reduces due to endothermic steam reforming. To compensate for this, the rotational speed of the recirculation blower  $\omega_{\text{rec}}$  can be increased. This allows the fuel inlet temperature to be stabilized and the system to be transferred to a steady-state operating point. In case the blower speed reaches the maximum value before stabilizing  $T''_{\text{fuel,R}}$ , the recirculation mass flow  $\dot{m}_{\text{rec}}$  can be further increased by increasing the system pressure  $p_{\text{sys}}$ . However, this leads to an increase in heat losses  $\dot{Q}_{\text{loss}}$  and thus to a lower required air mass flow  $\dot{m}_{\text{air}}$ . After heat losses and air mass flow stabilize, the system becomes stationary. However, if the air mass flow reaches its minimum value (preheater limitation or oxygen utilization) without stabilizing the temperature, the reactor temperature drops  $T_{\text{SOFC}}$ . This can be compensated by an increase in electrical power  $P_{\text{el}}$ , which in turn requires a higher recirculation mass flow. At one point, an additional power increase will not be possible as the minimum voltage  $U_{\text{cell,min}}$  will be reached and the operation is not possible and the methane share in the fuel needs to be reduced. This cycle can be broken by a wider range of operating parameters of the individual components or the usage of insulation materials that are not pressure dependent.

This shows that the combination of several potentially efficient features such as fuel gas recirculation and pressurization will not necessarily increase the system performance. Both pressurization and fuel gas recirculation have advantages and disadvantages. Pressurization increases the Nernst potential, decreases the polarization losses, and has advantages when integrating SOFC reactors into process systems. However, it increases the investment cost and may need sophisticated controls. Additionally, this work also shows that the heat losses increase. Fuel gas recirculation can increase the system efficiency as fuel preheating and water evaporation are not necessary. However, it decreases the Nernst potential, and as the experiments show, it can also increase the vertical temperature spread in an SOFC reactor. This leads to a lower average stack operating temperature with higher ohmic and polarization losses. SOFC reactors that are used in systems with recirculation should be designed for the high flows by using a different gas distribution approach in the sub-reactors. In case the recirculation only provides the water for the steam reforming and not the thermal energy,

the effect will be less strong. This could be achieved by an additional heat exchanger on the fuel side or by changing the reforming method to slightly autothermal.

## 4. Conclusions and Future Research

In this work, a commercially available 30 kW SOFC reactor with multiple stacks was operated. This was done within a pressurized system test rig equipped with a fuel gas recirculation device that operates at SOFC reaction temperature. Such a setup was investigated for the first time in the scientific community. The main objectives of the study were the analysis of the SOFC reactor operation behavior with respect to the individual stacks and the influence of the system components on the SOFC reactor.

### 4.1. Conclusions on Characteristics of SOFC Reactors with Multiple Stacks

This work showed the differences between the operation of cells and single stacks compared to reactors with multiple stacks. For the operation of SOFC reactors with multiple stacks, the following key points were highlighted: 1) An SOFC reactor with multiple stacks cannot be treated as a collection of equally behaving cells or stacks. The individual stacks operate under different operating conditions due to temperature, flow distribution, and heat losses. Therefore, such reactors have to be treated as a complex system of several sub-reactors, which are influenced by each other and their surroundings. For example, the average temperature difference between the stack with the highest and the stack with the lowest temperature was 50 K; 2) The maximum electrical power of an SOFC reactor with multiple stacks will be lower than the design power of its stacks. This will result in higher investment costs. However, this increase can be mitigated if the SOFC reactor's behavior is already considered during the system design; and 3) As the individual stacks will degrade at different rates due to the different operating conditions, SOFC reactors should be designed in such a way that an exchange of stacks is possible. Moreover, the operating strategies should try to minimize uneven degradation and should be able to operate unevenly degraded SOFC reactors efficiently.

The modular arrangement is responsible for the unequal flow distribution and thus the performance of the stacks. Newer SOFC reactors may show better flow and temperature distribution and have larger active cell areas. However, at least intermediate-future reactors will also consist of multiple individual stacks, which face the same challenges on a larger power scale to address the multi-megawatt range.

### 4.2. Conclusions on Integrated SOFC Systems

Furthermore, the impact of the system and its balance of plant components on the SOFC reactor was described. For the operation and design of SOFC systems, several key points were highlighted. 1) It was shown that combining several potentially efficient features such as fuel gas recirculation and pressurization does not generally increase system performance and robustness. For example, pressurization decreases the electrochemical losses but increases the system heat losses by more than

1 kW bar<sup>-1</sup>. Furthermore, the usage of a recirculation device to provide heat and water for steam reforming allows high reactant conversion but increases the cooling ratio of fuel and air to more than 1; 2) The difference in operation of cells, single stacks, and reactors with multiple stacks has to be considered during system design to evaluate the requirements of the system components; and 3) Complex control schemes that should increase system performance should not be designed based on models that represent only one cell or stack. Furthermore, controls that balance the sub-reactors in a large SOFC reactor should be developed.

### 4.3. Future Research

In the next measurement campaign, a detailed heat loss investigation will be conducted by varying pressure and vessel temperature to analyze the influence on the temperature distribution. By adding carbon dioxide to the fuel, operation with biogas will be analyzed. Finally, the preheater and the system pressure valve can be used to emulate the coupling with a gas turbine. For the detailed understanding of SOFC reactors with multiple stacks and their operation in process systems, a fast but detailed model of SOFC reactors with multiple stacks, based on the cell model presented by Srikanth et al.,<sup>[37]</sup> will be developed.<sup>[38]</sup> Both experiments on SOFC reactors and the proposed simulation model will be used to develop control and operation strategies for SOFC systems to increase their efficiency and robustness. Furthermore, it will be investigated to what extent the results can be transferred to electrolysis systems with SOCs.

### Supporting Information

Supporting Information is available from the Wiley Online Library or from the author.

### Acknowledgements

This project has received funding from the European Union's Horizon 2020 research and innovation program under grant agreement No 641073. Furthermore, the support from the German Federal Ministry of Economic Affairs and Energy for the project "DemoHydra" is gratefully acknowledged (support code: 03ET6032). The authors are responsible for the content of this publication.

Open access funding enabled and organized by Projekt DEAL.

### Conflict of Interest

The authors declare no conflict of interest.

### Data Availability Statement

Research data are not shared.

### Keywords

experiments, fuel gas recirculation, pressurization, reactors, SOFC, systems

Received: December 7, 2021

Revised: January 27, 2022

Published online: February 18, 2022

- [1] C. Geipel, K. Hauptmeier, K. Herbrig, F. Mittmann, M. Münch, M. Pötschke, L. Reichel, T. Strohbach, T. Seidel, A. Surrey, C. Walter, *ECS Trans.* **2019**, *91*, 123.
- [2] M. C. Williams, S. D. Vora, G. Jesionowski, *ECS Trans.* **2020**, *96*, 1.
- [3] M. Henke, J. Kallo, K. A. Friedrich, W. G. Bessler, *Fuel Cells* **2011**, *11*, 581.
- [4] A. Buonomano, F. Calise, M. D. d'Accadia, A. Palombo, M. Vicidomini, *Appl. Energy* **2015**, *156*, 32.
- [5] M. Henke, S. Hillius, M. Riedel, J. Kallo, K. A. Friedrich, *Fuel Cells* **2016**, *16*, 584.
- [6] M. Gandiglio, A. Lanzini, M. Santarelli, M. Acri, T. Hakala, M. Rautanen, *Int. J. Hydrogen Energy* **2020**, *45*, 5449.
- [7] P. Nehter, B. Wildrath, A. Bauschulte, K. Leites, *ECS Trans.* **2017**, *78*, 171.
- [8] S. Santhanam, D. Ullmer, Z. Wullemin, E. Varkaraki, C. Beetschen, Y. Antonetti, A. Ansar, *ECS Trans.* **2019**, *91*, 159.
- [9] J. Aicart, Z. Wullemin, B. Gervasoni, D. Reynaud, F. Waeber, C. Beetschen, Y. Antonetti, A. Nesci, J. Mougin, *Int. J. Hydrogen Energy* **2022**, *47*, 3568.
- [10] L. Bernadet, G. Gousseau, A. Chatroux, J. Laurencin, F. Mauvy, M. Reyrier, *Int. J. Hydrogen Energy* **2015**, *40*, 12918.
- [11] A. A. Burke, L. G. Carreiro, J. R. Izzo, *Int. J. Hydrogen Energy* **2013**, *38*, 13774.
- [12] S. H. Jensen, X. Sun, S. D. Ebbesen, M. Chen, *Fuel Cells* **2016**, *16*, 205.
- [13] A. Momma, K. Takano, Y. Tanaka, T. Kato, A. Yamamoto, *ECS Trans.* **2013**, *57*, 699.
- [14] M. Riedel, M. P. Heddrich, K. A. Friedrich, *Int. J. Hydrogen Energy* **2019**, *44*, 4570.
- [15] R. Peters, M. Frank, W. Tiedemann, I. Hoven, R. Deja, N. Kruse, Q. Fang, L. Blum, R. Peters, *J. Electrochem. Soc.* **2021**, *168*, <https://doi.org/10.1149/1945-7111/abdc79>.
- [16] P. H. Wagner, Z. Wullemin, D. Constantin, S. Diethelm, J. Van Herle, J. Schifmann, *Appl. Energy* **2020**, *262*, <https://doi.org/10.1016/j.apenergy.2019.114219>.
- [17] M. Henke, M. Steilen, C. Schnegelberger, M. Riedel, M. Hohloch, S. Bucheler, M. Herbst, A. Huber, J. Kallo, K. A. Friedrich, *ECS Trans.* **2015**, *68*, 85.
- [18] Y. Tanaka, K. Sato, A. Yamamoto, T. Kato, *ECS Trans.* **2013**, *57*, 443.
- [19] K. Sato, CAP Co. Ltd., Anode Gas Recycle Blower for SOFC, <http://www.cap-co.jp/SOFCE.html> (accessed: November 2020).
- [20] M. Henke, M. Tomberg, in *Deliverables of EU Projekt Biogas-fired Combined Hybrid Heat and Power Plant (Bio-HyPP)*, Vol. D2.5, German Aerospace Center (DLR), Stuttgart, Germany **2017**.
- [21] M. Henke, M. Steilen, R. Näke, M. P. Heddrich, K. A. Friedrich, in *12th European SOFC & SOE Forum*, Lucerne, Switzerland **2016**.
- [22] A. Marcellan, A. Abrassi, M. Tomberg, in *SUPEHR19 Sustainable PolyEnergy generation and HaRvesting*, Vol. 113, E3S Web of Conferences, Genoa, Italy **2019**.
- [23] J. G. Ziegler, N. B. Nichols, *ASME Trans.* **1942**, *64*, 759.
- [24] K. J. Åström, R. M. Murray, *Feedback Systems*, Princeton University Press, Princeton, NJ **2012**.
- [25] S. Santhanam, M. P. Heddrich, M. Riedel, K. A. Friedrich, *Energy* **2017**, *141*, 202.
- [26] A. Li, C. Song, Z. Lin, *Appl. Energy* **2017**, *190*, 1234.
- [27] M. Navasa, X.-Y. Miao, H. L. Frandsen, *Int. J. Hydrogen Energy* **2019**, *44*, 23330.

- [28] D. H. Kim, Y. Bae, S. Lee, J.-W. Son, J. H. Shim, J. Hong, *Energy Convers. Manage.* **2020**, 222, <https://doi.org/10.1016/j.enconman.2020.113213>.
- [29] L. A. Chick, O. A. Marina, C. A. Coyle, E. C. Thomsen, *J. Power Sources* **2013**, 236, 341.
- [30] M. Riedel, M. P. Heddrich, A. Ansar, Q. Fang, L. Blum, K. A. Friedrich, *J. Power Sources* **2020**, 475.
- [31] J. Brabandt, O. Posdziech, *ECS Trans.* **2017**, 78, 2987.
- [32] T. W. Clyne, I. O. Golosnoy, J. C. Tan, A. E. Markaki, *Philos. Trans. R. Soc., A* **2006**, 364, 125.
- [33] M. Kaviany, in *Handbook of Heat Transfer*, 3rd ed., (Eds: W. M. Rohsenow, J. P. Hartnett, Y. I. Cho), McGraw-Hill Education, New York City, USA **1998**.
- [34] R. Waitz, A. Wilfart, *Heat Process.* **2006**, 4, 207.
- [35] W. G. Bessler, *J. Electrochem. Soc.* **2006**, 153, A1492.
- [36] J. Nielsen, J. Hjelm, *Electrochim. Acta* **2014**, 115, 31.
- [37] S. Srikanth, M. P. Heddrich, S. Gupta, K. A. Friedrich, *Appl. Energy* **2018**, 232, 473.
- [38] M. Tomberg, S. Santhanam, M. P. Heddrich, A. Ansar, K. A. Friedrich, *ECS Trans.* **2019**, 91, 2089.